

# Continuum limit of lattice quasielectron wavefunctions

Aniket Patra, Birgit Hillebrecht, and Anne E. B. Nielsen\*

Max-Planck-Institut für Physik komplexer Systeme, D-01187 Dresden, Germany

The charged local anyonic excitations of the fractional quantum Hall effect – the quasihole and the quasielectron – are created by adding or removing a magnetic flux. The existing trial wavefunctions of the quasielectron have several problems, such as lack of screening or wrong braiding properties. It was shown, however, that for lattice fractional quantum Hall systems, it is possible to find a relatively simple quasielectron wavefunction that has all the desired properties [New J. Phys. 20, 033029 (2018)]. This naturally poses the question: what happens to this wavefunction in the continuum limit? Here we demonstrate that, although one obtains a finite continuum wavefunction when the quasielectron is on top of a lattice site, such a limit of the lattice quasielectron does not exist in general. In particular, if the quasielectron is put anywhere else than on a lattice site, the lattice wavefunction diverges when the continuum limit is approached. The divergence can be removed by projecting the state on the lowest Landau level, but we find that the projected state does also not have the desired properties. We hence conclude that the lattice quasielectron wavefunction does not solve the difficulty of finding good trial states for quasielectrons in the continuum.

## I. INTRODUCTION

The discovery of the fractional quantum Hall effect (FQHE) in heterojunctions in solids [1] marks the genesis of the enduring interest in strongly correlated topologically ordered systems [2–4]. The topology in the FQHE is manifested in the presence of quasiholes and quasielectrons, which are anyonic excitations with positive and negative charge, respectively. In such solid-state systems [1], similar experimental manipulations – increasing or decreasing the external magnetic field – lead to realizations of quasiholes or quasielectrons, respectively.

Kitaev pointed out the usefulness of anyons in fault-tolerant topological quantum computing [5]. The first step in achieving this, by utilizing the anyonic excitations appearing in the FQHE, is to theoretically understand them. The dimension of such systems' Hilbert space being exponential in the number of electrons renders it difficult for obtaining numerical results *ab initio*. Descriptions in terms of ansatz wavefunctions have traditionally provided the way forward.

For example, Laughlin provided an ansatz wavefunction explaining the FQHE ground state at  $1/3$  filling [6]. In the same paper, he also provided an ansatz for the quasihole excitation, where the electron density is locally decreased, by modifying the ground state wavefunction. However, the difficulty of obtaining an ansatz for the quasielectron, where the electron density at the location of the quasielectron needs to be increased, was immediately understood. This leads to a pole singularity due to the Pauli exclusion principle.

Distinct wavefunctions for quasiholes and quasielectrons in the FQHE with different filling fractions were introduced using several different approaches [6–16]. Laughlin, in his paper, introduced an ansatz in terms of derivative operators  $\partial/\partial Z_i$ , where  $Z_i$  are the electron coordinates [6]. Under the composite fermion framework, Jeon and Jain proposed a different ansatz that has lower variational energy compared to the

Laughlin ansatz [8]. This quasielectron ansatz can be thought of as a composite of a quasiparticle of negative charge  $-2/3$  and a quasihole of charge  $1/3$ , orbiting around the common center of mass with positive relative angular momentum [9]. One can obtain a quasielectron wavefunction by using a physical clustering condition, where it must vanish when certain patterns of clusters of electrons are formed [10]. Another way to obtain quasielectron and quasihole ansätze is to consider correlation functions of certain rational CFTs that involve nonlocal operators [11–13]. How to construct all states in the Abelian quantum Hall hierarchy using the above quasihole and quasielectron wavefunctions was also explained [14]. An operator formalism describing the Laughlin quasielectron in FQH systems with periodic boundary conditions (i.e., on a 2-torus) is also known [15]. In all these descriptions, however, there are problems with wrong braiding statistics or that the quasielectron is not necessarily at the right position. A description without these problems was found in [16], but it required some *ad hoc* modifications to obtain the expected density profiles numerically.

It is possible to write trial wavefunctions for quasiholes and quasielectrons on a lattice [17], which do not suffer from the aforementioned shortcomings. This description is particularly simple because the quasiparticle operators are written in terms of a single screened chiral boson field, and the density profiles are undistorted due to absence of additional screening requirements. Interesting strongly correlated topological phases such as topological Chern insulators are only present in such lattice systems [18–20]. These are, e.g., relevant for implementations in optical lattices. In this paper, we investigate the continuum limit of these lattice wavefunctions. This analysis of the continuum limit – necessary for the description of solid-state anyonic excitations – was absent in Ref. [17]. Although placing the quasielectron on a lattice site produces a finite trial wavefunction, our analytical calculations show that the continuum limit of the quasielectron does not exist in general. Additionally, we show that an attempt to cure the wavefunction of this problem by projecting it on the lowest Landau level (LLL) in the continuum limit, as was alluded to in [6], is unphysical. In particular, the LLL-projected continuum quasielectron ansatz does not have the right braiding properties.

\* On leave from Department of Physics and Astronomy, Aarhus University, DK-8000 Aarhus C, Denmark

We recapitulate the Laughlin wavefunctions for the continuum FQH ground state and the quasi-hole in Sect. II, and explain why the quasi-electron – described as an inverse quasi-hole – is singular. We recall in Sect. III the wavefunctions for the anyonic excitations on a lattice with  $N$  lattice points. These wavefunctions are not singular for finite  $N$ . In Sect. IV A, we approach the continuum limit by increasing the number of the lattice points  $N$ , while keeping the number of electrons and the number of magnetic fluxes in the system constant. We consider different positions of the quasi-electron in relation to the lattice sites. In particular, we explain that, when we put the quasi-electron on top of a lattice site, it leads to a finite trial wavefunction. In Sect. IV B, we identify the terms that diverge in the continuum limit. We show that the ratio of the contributions from the divergent and regular terms is proportional to  $\ln N$ . This means that the continuum quasi-electron is singular and is not confined to the LLL. The slow nature of this divergence makes it hard for detection in the numerics. We numerically show that indeed only the divergent terms are responsible for bringing about the most amount of change in the physical observables (e.g., excess charge) as we approach the continuum limit.

To remove the singularity we project the quasi-electron on the LLL. We study this modified divergence free ansatz in Sect. V, and explain how this also does not possess the desired properties. In Sect. V A 1 we show that the anyon statistics obtained by moving a LLL-projected quasi-electron adiabatically around a quasi-hole is different from the one obtained by moving the quasi-hole around the same quasi-electron. The Berry phase obtained by moving the LLL-projected quasi-electron around a quasi-hole depends on the size and shape of the contour. Moreover, in Sect. V A 2, we demonstrate that, if starting from the ansatz wavefunction with a quasi-hole and a LLL-projected quasi-electron we take the position of the quasi-electron to infinity, we fail to retrieve the wavefunction for an isolated quasi-hole.

## II. LAUGHLIN WAVEFUNCTION: CONTINUUM DESCRIPTION

Consider a FQH droplet of filling fraction  $1/q$  with  $M$  electrons, where  $q$  is a positive integer. To describe  $K$  quasiparticles at  $w_1, \dots, w_K$ , Laughlin introduced the following ansatz wavefunctions:

$$|\psi\rangle_{\text{cont}} = \mathcal{C}^{-1} \int \dots \int \prod_{i=1}^M d^2 Z_i |Z_1, \dots, Z_M\rangle \times \prod_{i,k} (w_k - Z_i)^{p_k} \prod_{i<j} (Z_i - Z_j)^q e^{-\sum_{i=1}^M |Z_i|^2 / 4l_B^2}, \quad (1)$$

where  $\mathcal{C}$  is a real normalization constant, the electronic coordinates  $Z_i$  take any value on the complex plane, and  $l_B$  is the magnetic length [6]. The Jastrow factor prevents two particles from being at the same position. The state describes fermions for  $q$  odd and hardcore bosons for  $q$  even.

There are two types of quasiparticles in the FQHE, namely the quasi-hole and the quasi-electron with fractional charges

$+e/q$  and  $-e/q$ , respectively. Here  $e > 0$  is the absolute value of the electronic charge. In Eq. (1),  $p_k = 0$  for all  $k$ , produces the Laughlin FQHE ground state wavefunction. When  $p_k = +1$ , there is a quasi-hole at  $w_k$ , where the additional (local in  $w_k$ ) factor  $\prod_i (w_k - Z_i)$  corresponds to the insertion of a positive flux tube at  $w_k$  [6].

However, the wavefunction is not physical when  $p_k = -1$ . The factor corresponding to the insertion of a negative flux tube at  $w_k$  is singular, when any of the electronic coordinates  $Z_i$  are equal to  $w_k$ . This renders the naive description of the quasi-electron to be an inverse quasi-hole invalid.

## III. LATTICE WAVEFUNCTIONS

In this section, we recall the salient features of the quasi-electron wavefunction on a lattice, which was introduced in Ref. [17]. The lattice sites are  $z_i$  for  $i = 1, \dots, N$ . Here we consider the case of a square lattice with a roughly circular boundary of radius  $R$ . The local basis on site  $i$  is labelled by  $|n_i\rangle$ , where the lattice occupancy  $n_i$  is either 0 or 1. After setting the magnetic length  $l_B = 1$ , it is possible to write down the wavefunction for  $K$  different quasiparticles at the positions  $w_1, \dots, w_K$  in terms of the chiral correlator of CFT vertex operators as follows:

$$|\psi\rangle \propto \sum_{n_1, \dots, n_N} \langle 0 | \prod_{k=1}^K W_{p_k} \prod_{i=1}^N V_{n_i} | 0 \rangle |n_1, \dots, n_N\rangle, \quad (2)$$

where the vertex operators are

$$W_{p_k} = : e^{ip_k \phi(w_j) / \sqrt{q}} :, \quad (3)$$

$$V_{n_j} = \chi_{n_j} : e^{i(qn_j - \eta)\phi(z_j) / \sqrt{q}} :.$$

Here  $: \dots :$  denotes normal ordering,  $\phi(z_j)$  is the chiral field of a massless free boson evaluated at the position  $z_j$ ,  $\chi_{n_j}$  are the unspecified single particle phase factors that do not depend on the  $w_j$ , and the area assigned per single lattice site is  $2\pi\eta$ . The vertex operator  $W_{p_k}$  with  $p_k = +1$  ( $-1$ ) creates a quasi-hole (quasi-electron).

From Eq. (2), we obtain the following ansatz for the  $K$  quasiparticle excitations at the positions  $w_1, \dots, w_K$ :

$$|\psi\rangle = \mathcal{C}^{-1} \sum_{n_1, \dots, n_N} \delta_n \prod_{i=1}^N \chi_{n_i} \prod_{i,k} (w_k - z_i)^{p_k n_i} \times \prod_{i<j} (z_i - z_j)^{qn_i n_j - \eta(n_i + n_j)} |n_1, \dots, n_N\rangle. \quad (4)$$

Note that the correlation function is zero unless the charge neutrality condition,

$$\sum_{i=1}^N n_i = \left( \eta N - \sum_{k=1}^K p_k \right) / q, \quad (5)$$

is obeyed by the lattice occupancies. This is imposed in Eq. (4) by the Kronecker delta function  $\delta_n$ . The real normalization constant  $\mathcal{C}$  in Eq. (4) is a function of the quasiparticle positions, and it obeys

$$\begin{aligned} \mathcal{C}^2 &= \sum_{n_1, \dots, n_N} \delta_n \prod_{k,j} |w_k - z_j|^{2p_k n_j} \\ &\quad \times \prod_{i < j} |z_i - z_j|^{2q n_i n_j - 2\eta(n_i + n_j)} \\ &= \sum_{n_1, \dots, n_N} \delta_n \mathcal{C}_{n_1, \dots, n_N}^2. \end{aligned} \quad (6)$$

Eq. (4) provides a valid (finite) trial wavefunction. This ansatz also works when the quasielectron position  $w_k$  is arbitrarily close to a lattice site  $z_i$ . In this case, the proximity of  $w_k$  and  $z_i$  forces  $n_i \rightarrow 1$ . This allows us to include the infinitely large constant  $(w_k - z_i)^{-1}$  in the normalization.

The charge neutrality condition described in Eq. (5) guarantees that the number of particles in the FQH droplet remains constant for any  $\eta$ . This in turn means  $N\eta = \text{constant}$ , where  $N$  is the number of lattice sites inside the circle of fixed radius  $R$ . As we decrease  $\eta$ ,  $R$  stays fixed, but the number of sites inside the circle increases, which allows the particles to be in more places. Thus the parameter  $\eta$  allows us to interpolate between the lattice limit ( $\eta = 1$ ) and the continuum limit ( $\eta \rightarrow 0^+$ ). In the continuum limit and with  $p_k = 0$  for all  $k$ , starting from the wavefunction (4) defined on a lattice with uniformly distributed sites and a circular boundary, one obtains the Laughlin wavefunction. In the continuum limit, the occupied subset of lattice points ( $M$  of them) are the electronic coordinates  $Z_1, \dots, Z_M$  [21].

### A. Braiding Statistics

When the  $k$ th anyon situated at  $w_k$  moves adiabatically in a closed contour  $c$ , the wavefunction is modified as  $|\psi\rangle \rightarrow \mathbb{M} e^{i\theta_k} |\psi\rangle$ . Here  $\theta_k$  is the Berry phase, and the monodromy  $\mathbb{M}$  is the change in the wavefunction effected by only the analytical continuation.

For future use, we briefly repeat the computation of the Berry phase  $\theta_k$ . Starting with the wavefunction (4) for  $K$  anyons, we write  $\theta_k$  as follows:

$$\begin{aligned} \theta_k &= i \oint_c \left\langle \psi \left| \frac{\partial \psi}{\partial w_k} \right. \right\rangle dw_k + \text{c.c.} \\ &= \frac{i}{2} \oint_c \frac{1}{\mathcal{C}^2} \frac{\partial \mathcal{C}^2}{\partial w_k} dw_k + \text{c.c.} \end{aligned} \quad (7)$$

From Eq. (6) we observe that

$$\frac{\partial \mathcal{C}^2}{\partial w_k} = \sum_{n_1, \dots, n_N} \delta_n \mathcal{C}_{n_1, \dots, n_N}^2 \sum_j \frac{p_k n_j}{w_k - z_j}. \quad (8)$$

We also recall the following expression for the expectation value of an operator  $\hat{O}$  that is diagonal in the  $|n_1, \dots, n_N\rangle$  basis:

$$\begin{aligned} \langle \psi | \hat{O} | \psi \rangle &= \frac{1}{\mathcal{C}^2} \sum_{n_1, \dots, n_N} \delta_n \mathcal{C}_{n_1, \dots, n_N}^2 \\ &\quad \times \langle n_1, \dots, n_N | \hat{O} | n_1, \dots, n_N \rangle. \end{aligned} \quad (9)$$

Using Eqs. (7), (8), and (9), we obtain [22, 23]

$$\theta_k = i \frac{p_k}{2} \oint_c \sum_i \frac{\langle n_i \rangle}{w_k - z_i} dw_k + \text{c.c.} \quad (10)$$

When the quasiparticles are screened – i.e., a quasiparticle at  $w_j$  only affects the particle densities close to  $w_j$  (see Fig. 2, for example) – it is possible to separate them sufficiently. We now move a quasiparticle at  $w_k$  in a closed contour  $c$ , such that  $w_j$  always remains far from  $c$ . One then writes the anyonic statistics  $\gamma$  of the  $k$ th and the  $j$ th quasiparticles as

$$\begin{aligned} 2\pi\gamma &= \theta_{k, (w_j \text{ inside})} - \theta_{k, (w_j \text{ outside})} \\ &= \frac{ip_k}{2} \oint_c \sum_i \frac{\langle n_i \rangle_{(w_j \text{ inside})} - \langle n_i \rangle_{(w_j \text{ outside})}}{w_k - z_i} dw_k \\ &\quad + \text{c.c.}, \end{aligned} \quad (11)$$

where  $\theta_{k, (w_j \text{ inside})}$  ( $\theta_{k, (w_j \text{ outside})}$ ) is the Berry phase with the  $j$ th anyon inside (outside)  $c$ . In the above equation, we have used the fact that the monodromy  $\mathbb{M}$  is the identity.

For screened and well-separated anyons,  $\langle n_i \rangle_{(w_j \text{ inside})} - \langle n_i \rangle_{(w_j \text{ outside})}$  is independent of  $w_k$ . It is non-zero only for lattice positions that are close to the two possible values of  $w_j$ . Using this in Eq. (11), one obtains the correct anyon statistics:  $\gamma = p_j p_k / q$ . We note that the above argument neither depends on the nature (whether they are quasiholes or quasielectrons) of the anyons, nor on the value of  $\eta$ .

## IV. DIVERGENCE OF THE CONTINUUM LIMIT OF THE LATTICE WAVEFUNCTION

For the sake of definiteness, we consider one quasielectron at  $w_1$  and one quasihole at  $w_2$ . We write the ansatz for this system using Eq. (4) as follows:

$$\begin{aligned} |\psi\rangle &= \mathcal{C}^{-1} \sum_{n_1, \dots, n_N} \delta_n \prod_{i=1}^N \chi_{n_i} \prod_{i=1}^N \left( \frac{w_2 - z_i}{w_1 - z_i} \right)^{n_i} \\ &\quad \times \prod_{i < j} (z_i - z_j)^{q n_i n_j - \eta(n_i + n_j)} |n_1, \dots, n_N\rangle. \end{aligned} \quad (12)$$

Note that, since  $\sum_k p_k = 0$  in this system, we still have  $M = N\eta/q$  particles.

### A. Continuum Limit of the Quasielectron Ansatz: Numerics

In order to isolate and study the properties of the quasielectron, we consider  $w_1$  to be the origin and  $w_2$  to be the complex infinity. In the limit  $w_2 \rightarrow \infty$ , the factor  $\prod_{i=1}^N (w_2 - z_i)^{n_i}$  approaches  $\prod_{i=1}^N w_2^{n_i} = w_2^M$ , which is a constant (albeit, an infinite one) that can be absorbed in the normalization. This gives the following wavefunction for a single quasielectron:

$$|\psi_{\text{QE}}\rangle = \mathcal{C}^{-1} \sum_{n_1, \dots, n_N} \delta_n \prod_{i=1}^N \tilde{\chi}_{n_i} \prod_{i=1}^N z_i^{-n_i}$$



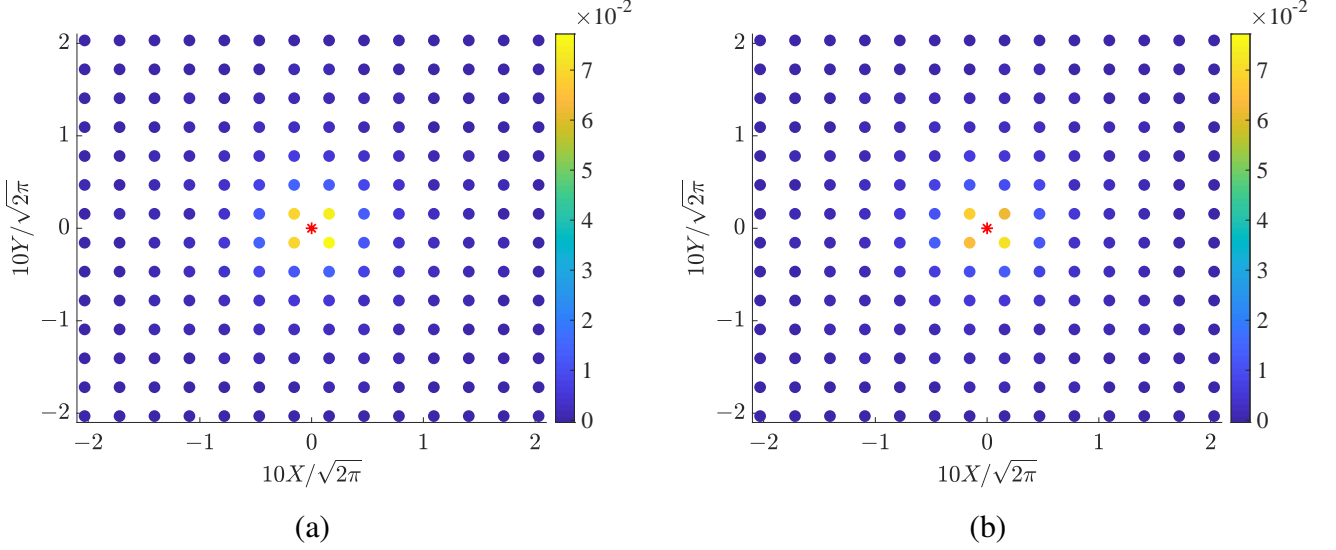


FIG. 2. Excess particle densities  $\langle n_i \rangle_{-1} - \langle n_i \rangle_0$  (see below Eq. (17) for the definitions of  $\langle n_i \rangle_{-1}$  and  $\langle n_i \rangle_0$ ) at different lattice points in the presence of a quasielectron (13), shown by the red star at the origin, for inverse filling fractions  $q = 2$  (a), and  $q = 3$  (b). Here we only show a part of the lattice. The particle densities of only a few lattice sites close to the quasielectron are affected. The screened nature of the quasielectron proves that the quasiparticles described by Eq. (4) have the correct braiding properties, see Sect. III A.

### B. Divergence of the Continuum Quasielectron: Analytical Argument

The foregoing numerical calculation could not definitively answer if the quasielectron (13) leads to a singularity in the continuum, when it is placed at the center of a square plaquette or midway between two lattice points. We therefore take recourse to an analytical argument. When we are close to the continuum limit, there are so many lattice points that the electrons can be almost anywhere. However, at the place where we have the singularity, the difference between the lattice and the continuum is important.

In particular, the underlying lattice structure introduces a distance of closest approach from the quasielectron position  $\xi$  (as long as the quasielectron is not placed on top of a lattice point). Since the length of the primitive lattice vectors in the square lattice is  $\sqrt{2\pi\eta}$ , we have

$$\xi \propto \sqrt{\eta} \propto 1/\sqrt{N}. \quad (18)$$

The proportionality constant in Eq. (18) depends on the position of the quasielectron with respect to a square plaquette.

In the continuum, the LLL is well-defined and the quasielectron should be entirely confined to it. This does not hold for the wavefunction (13) because of the  $1/z_i$  factors. We write the norm of the single electron LLL wavefunction  $e^{-|Z|^2/4}$  multiplied by the quasielectron pole  $1/Z$  over a domain with a hole around the singularity as follows:

$$\begin{aligned} & \iint_{D'} \left| \frac{e^{-|Z|^2/4}}{Z} \right|^2 d^2Z \\ &= \iint_D \Theta^2(|Z| - \xi) \left| \frac{e^{-|Z|^2/4}}{Z} \right|^2 d^2Z, \end{aligned} \quad (19)$$

where  $\Theta(x)$  is the Heaviside step function (17). We perform the integral in the left hand side on a sufficiently large disk  $D$  with a small hole of radius  $\xi$  around the position of the quasielectron – the origin. We denote this not-simply-connected domain as  $D'$ . The integral on the right hand side, with the wavefunction  $\Theta(|Z| - \xi) e^{-|Z|^2/4}/Z$ , is performed on the full disk. The wavefunctions in both sides of Eq. (19) do not live in the LLL.

The preceding discussion establishes that the lattice quasielectron (13) tends to the following continuum quasielectron living on  $D'$ :

$$\begin{aligned} |\psi_{\text{QE}}\rangle_{\text{cont}} &= C^{-1} \int \cdots \int_{D'^M} \prod_{i=1}^M d^2Z_i |Z_1, \dots, Z_M\rangle \\ &\times \prod_i Z_i^{-1} \prod_{i<j} (Z_i - Z_j)^q e^{-\sum_{i=1}^M |Z_i|^2/4l_B^2}. \end{aligned} \quad (20)$$

Expanding the product  $\prod_{i<j} (Z_i - Z_j)^q$ , we write the wavefunction (20) as follows:

$$\begin{aligned} |\psi_{\text{QE}}\rangle_{\text{cont}} &= C^{-1} \int \cdots \int_{D'^M} \prod_{i=1}^M d^2Z_i |Z_1, \dots, Z_M\rangle \\ &\times \sum_{q_1, \dots, q_M} \mathcal{E}_{q_1, \dots, q_M} \prod_{l=1}^M Z_l^{q_l-1} e^{-|z_l|^2/4}, \end{aligned} \quad (21)$$

where  $\mathcal{E}_{q_1, \dots, q_M}$  are different expansion coefficients, and  $q_1, \dots, q_M$  satisfy

$$\sum_l q_l = qM(M-1)/2, \quad 0 \leq q_l \leq (M-1)q. \quad (22)$$

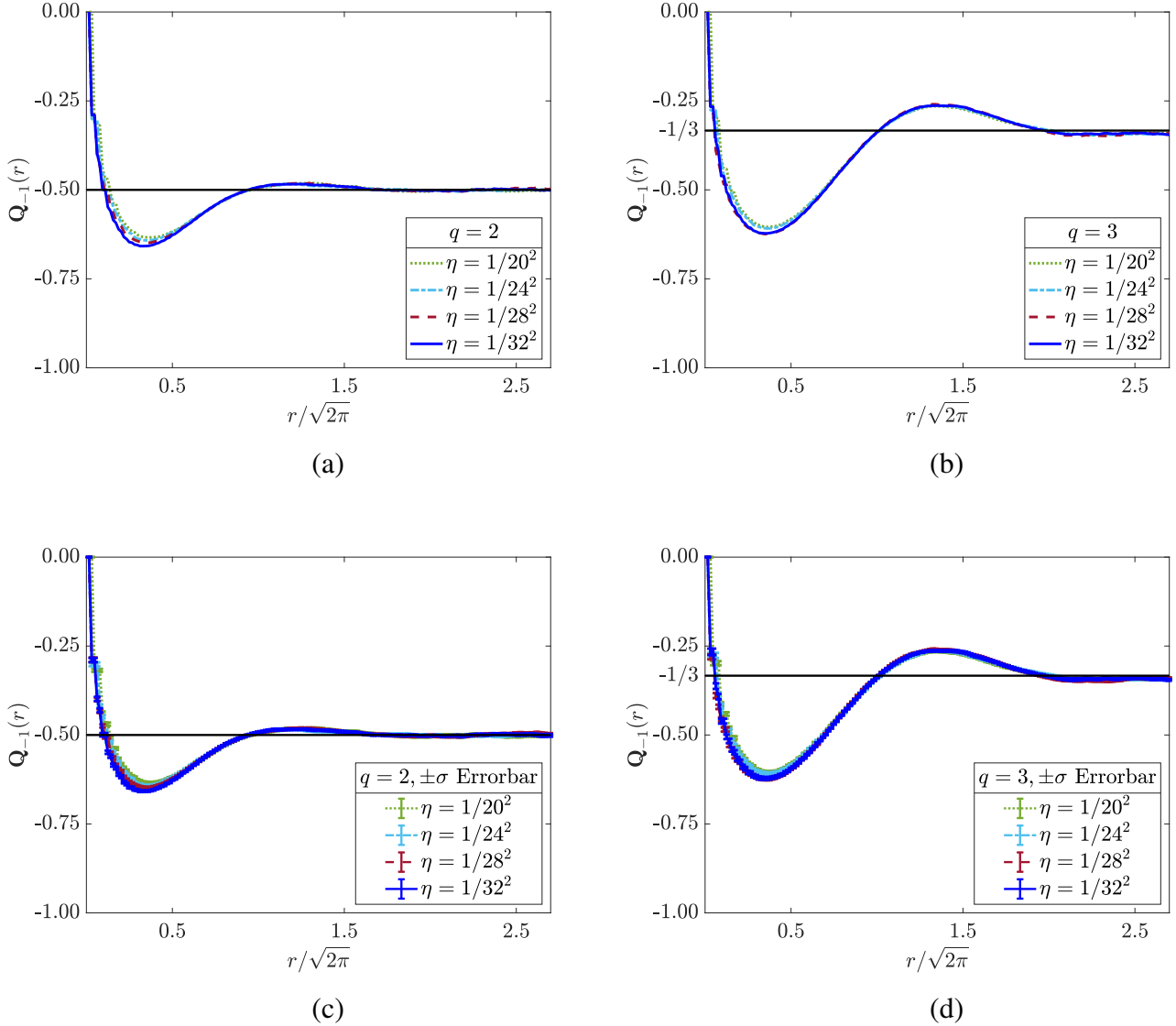


FIG. 3. Excess charge  $\mathbf{Q}_{-1}(r)$  of the quasielectron (13) for inverse filling fractions  $q = 2$  [(a) and (c)] and  $q = 3$  [(b) and (d)]. The quasielectron is at the origin of a circular disk of radius  $R \approx 5.6\sqrt{2\pi}$  with a square lattice with  $N$  lattice points embedded on it. We define  $\mathbf{Q}_{-1}(r)$  as a function of the radial distance  $r$  from the quasielectron in the units of absolute electronic charge  $e$  in Eq. (16). We show the  $\mathbf{Q}_{-1}(r)$  averaged over 25 different Monte Carlo datasets in (a) and (b). Additionally, in (c) and (d), we include an errorbar of  $\pm\sigma$  for the excess charge profiles, where  $\sigma$  is the variance of  $\mathbf{Q}_{-1}(r)$ . To approach the continuum, starting from the lattice limit  $\eta = 1$ , in consecutive steps we decrease  $\eta$  as  $\eta = 1/L^2$ , and put  $L^2N$  lattice sites on the same circular disk of radius  $R$ . We show the  $\mathbf{Q}_{-1}(r)$  profiles for  $L = 20, 24, 28$ , and  $32$ . For  $r \gtrsim 2\sqrt{2\pi}$ , for all the  $\eta$  values shown here, the excess charge for the quasielectron at filling fractions  $1/q$  is indeed close to  $1/q$ . When  $r$  is small, i.e., near the trough of the excess charge profile,  $\mathbf{Q}_{-1}(r)$  goes down as we decrease  $\eta$ . It is hard to conclude if the profile has reached a limit or not after including the  $\pm\sigma$  errorbar. In Sect. IV B, we argue that the curves do not converge.

Note that  $\mathcal{E}_{q_1, \dots, q_M}$  are the same coefficients that appear in the expansion of the Laughlin wavefunction (Eq. (1) with all  $p_k = 0$ ) in the basis  $|q_1, \dots, q_M\rangle$  of single electron wavefunction product, which we write as follows:

$$|\psi\rangle = \mathcal{C}^{-1} \sum_{q_1, \dots, q_M} \mathcal{E}_{q_1, \dots, q_M} |q_1, \dots, q_M\rangle. \quad (23)$$

To go back to the coordinate basis  $|Z_1, \dots, Z_M\rangle$ , one needs

to insert the following identity operator,

$$\mathbb{1} = \int \cdots \int_{D^M} \prod_{i=1}^M d^2 Z_i |Z_1, \dots, Z_M\rangle \langle Z_1, \dots, Z_M|, \quad (24)$$

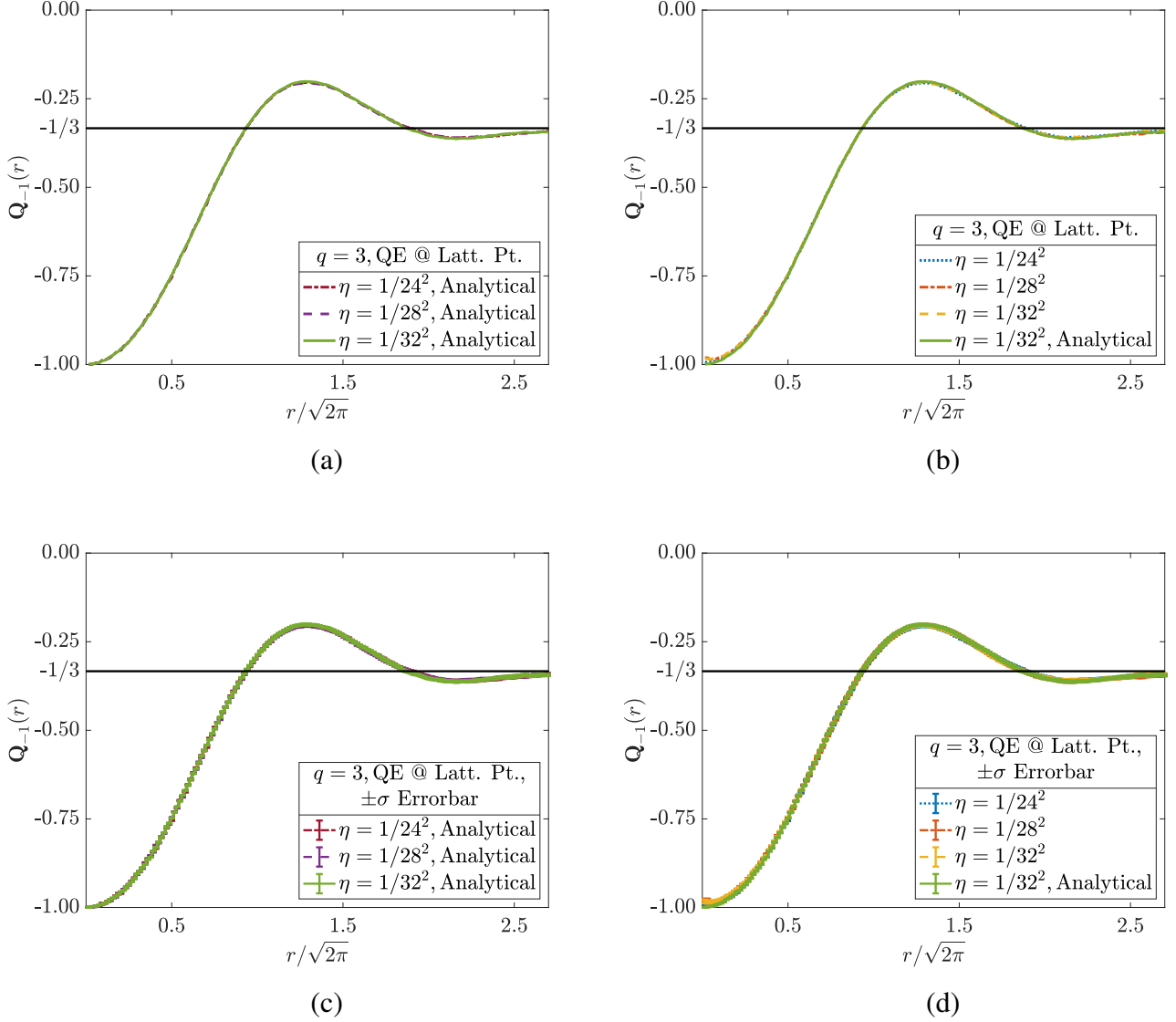


FIG. 4. Excess charge  $\mathbf{Q}_{-1}(r)$  profile with the quasielectron on a lattice site for  $q = 3$ . In (a), we plot  $\mathbf{Q}_{-1}(r)$  for  $\eta = 1/24^2$ ,  $1/28^2$ , and  $1/32^2$  using the exact analytical wavefunction, where we always keep the lattice site at  $\sqrt{2\pi\eta}(1/2, 1/2)$  occupied. The convergence of  $\mathbf{Q}_{-1}(r)$  is clearly demonstrated here. In (b), we compare the excess charge profile for  $\eta = 1/32^2$  obtained from the analytical wavefunction to the ones, with  $\eta = 1/24^2$ ,  $1/28^2$ , and  $1/32^2$ , obtained from the wavefunction with the quasielectron close to a lattice site at  $w = \sqrt{2\pi}(\sqrt{\eta}/2, \sqrt{\eta}/2 - 10^{-4})$ . In (c) and (d), we show (a) and (b) with  $\pm\sigma$  errorbars, respectively.

in Eq. (23), and use

$$\langle Z_1, \dots, Z_M | q_1, \dots, q_M \rangle \propto \prod_{l=1}^M Z_l^{q_l} e^{-\frac{|Z_l|^2}{4}}. \quad (25)$$

Using this, we write Eq. (21) as:

$$|\psi_{\text{QE}}\rangle_{\text{cont}} = \mathcal{C}^{-1} \sum_{q_1, \dots, q_M} \mathcal{E}_{q_1, \dots, q_M} |q_1 - 1, \dots, q_M - 1\rangle, \quad (26)$$

where  $|q_1 - 1, \dots, q_M - 1\rangle$  is an orthonormal product basis similar to  $|q_1, \dots, q_M\rangle$ . This new single electron basis on  $D'$ ,

however, includes the element  $|-1\rangle$  with

$$\langle Z | -1 \rangle \propto Z^{-1} e^{-\frac{|Z|^2}{4}}, \quad (27)$$

to accommodate the quasielectron pole. Note that the function (27) is normalizable on the domain  $D'$ .

We have two types of terms in the expansion (21) – the ones with all the  $q_i$  positive, and the ones with at least one of them equal to zero. The first type of terms  $\{q_1^{\text{reg}}, \dots, q_M^{\text{reg}}\}$  do not lead to any singularity. We delineate this regular (not normalized) part of the continuum quasielectron wavefunction (21) as follows:

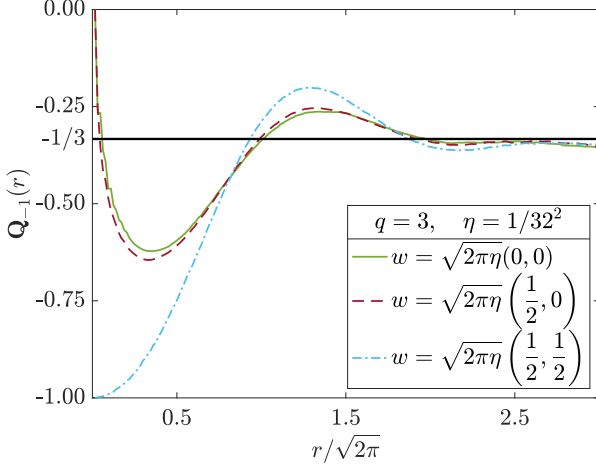


FIG. 5. Excess charge profiles for  $q = 3$  and  $\eta = 1/32^2$  with three different inequivalent positions  $w$  of the quasielectron in the square lattice. Here  $r$  is the radial distance from the quasielectron position. The three positions – center of a square plaquette (solid green), midpoint of a side (brown dashed), and on top of a lattice site (indigo dash-dot) – lead to different  $\mathbf{Q}_{-1}(r)$  profiles.

$$|\psi_{\text{QE}}^{\text{reg}}\rangle_{\text{cont}} = \mathcal{C}^{-1} \int \cdots \int_{D',M} \prod_{i=1}^M d^2 Z_i |Z_1, \dots, Z_M\rangle \times \sum_{q_1^{\text{reg}}, \dots, q_M^{\text{reg}}} \mathcal{E}_{q_1^{\text{reg}}, \dots, q_M^{\text{reg}}} \prod_{l=1}^M Z_l^{q_l^{\text{reg}}-1} e^{-\frac{|Z_l|^2}{4}}, \quad (28)$$

where  $\mathcal{C}$  is the same as in Eqs. (20) and (21).

The second type of terms  $\{q_1^\infty, \dots, q_M^\infty\}$  however, have at least one pole at the origin. Among all these terms, those that have poles of the type  $Z_k^{-1}$ , must have  $q_k = 0$  in Eq. (21). Factors of  $Z_k$  appear in  $\prod_{i<j} (Z_i - Z_j)^q$  either from  $\prod_{l(<k)} (Z_l - Z_k)^q$ , or from  $\prod_{l(>k)} (Z_k - Z_l)^q$ . Note that both the binomial expansions of  $(Z_l - Z_k)^q$  and  $(Z_k - Z_l)^q$  produce homogeneous polynomials of degree  $q$ . The only monomial in these expansions with no powers of  $Z_k$  is  $Z_l^q$ . This also shows that it is not possible to have two  $q_l$  to be equal to zero.

Using this we write the singular (not normalized) part of the continuum quasielectron wavefunction (20) as follows:

$$|\psi_{\text{QE}}^\infty\rangle_{\text{cont}} = \mathcal{C}^{-1} \int \cdots \int_{D',M} \prod_{i=1}^M d^2 Z_i |Z_1, \dots, Z_M\rangle \times \sum_{k=1}^M Z_k^{-1} \prod_{l(<k)} Z_l^{q_l-1} \prod_{l(>k)} (-Z_l)^{q_l-1} \prod_{\substack{i<j \\ i,j \neq k}} (Z_i - Z_j)^q \times e^{-\frac{|Z_j|^2}{4}}, \quad (29)$$

where  $\mathcal{C}$  is the same as in Eqs. (20), (21), and (28). After cancellation only one of these poles in  $\prod_l Z_l^{-1}$  remain in the singular terms (29). The other poles coming from  $\prod_{l(\neq k)} Z_l^{-1}$ ,

in the term that has a residual pole  $Z_k^{-1}$ , reduce the power of  $Z_l$  from  $q$  to  $q-1$ . Denoting the  $\{q_1^\infty, \dots, q_M^\infty\}$  with  $q_k = 0$  as  $\{q_1^{k_\infty}, \dots, q_M^{k_\infty}\}$  we finally write Eq. (29) as follows:

$$|\psi_{\text{QE}}^\infty\rangle_{\text{cont}} = \mathcal{C}^{-1} \int \cdots \int_{D',M} \prod_{i=1}^M d^2 Z_i \times |Z_1, \dots, Z_M\rangle \sum_{k=1}^M Z_k^{-1} \times \sum_{q_1^{k_\infty}, \dots, q_M^{k_\infty}} \mathcal{E}_{q_1^{k_\infty}, \dots, q_M^{k_\infty}} \prod_{l(\neq k)} Z_l^{q_l^{k_\infty}-1} e^{-\frac{|Z_l|^2}{4}}. \quad (30)$$

Using the orthogonality of the basis elements in the right hand side of Eq. (26), and Eqs. (28) and (30), we derive the following normalization condition for the wavefunction (21):

$$\mathcal{C}_{\text{reg}}^2 + \mathcal{C}_\infty^2 = \mathcal{C}^2, \quad (31)$$

where

$$\mathcal{C}_{\text{reg}}^2 = \sum_{q_1^{\text{reg}}, \dots, q_M^{\text{reg}}} \mathcal{E}_{q_1^{\text{reg}}, \dots, q_M^{\text{reg}}}^2 \prod_{l=1}^M \iint_{D'} d^2 Z_l \times |Z_l|^{2(q_l^{\text{reg}}-1)} e^{-\frac{|Z_l|^2}{2}}, \quad (32a)$$

$$\mathcal{C}_\infty^2 = \sum_{k=1}^M \iint_{D'} d^2 Z_k \frac{1}{|Z_k|^2} e^{-\frac{|Z_k|^2}{2}} \times \sum_{q_1^{k_\infty}, \dots, q_M^{k_\infty}} \mathcal{E}_{q_1^{k_\infty}, \dots, q_M^{k_\infty}}^2 \prod_{l(\neq k)} \iint_{D'} d^2 Z_l \times |Z_l|^{2(q_l^{k_\infty}-1)} e^{-\frac{|Z_l|^2}{2}}. \quad (32b)$$

The integrands of the type  $|Z_l|^{2(q_l-1)} e^{-\frac{|Z_l|^2}{2}}$  lead to the following radial integrals:

$$\int_0^\infty r_l^{2q_l-1} e^{-r_l^2/2} dr = 2^{q_l-1} \Gamma(q_l), \quad (33)$$

where in the  $\xi \rightarrow 0$  limit we have simply replaced  $\xi$  by zero. The integrands of the type  $|Z_k|^{-2} e^{-\frac{|Z_k|^2}{2}}$  in Eq. (32b), on the other hand, lead to

$$\int_\xi^\infty \frac{1}{r} e^{-r^2/2} dr = \frac{1}{2} E_1\left(\frac{\xi^2}{2}\right), \quad (34)$$

where  $\xi \propto 1/\sqrt{N}$  is the distance of closest approach between the electrons and the singularity, and  $E_1(x)$  is the exponential integral [24]. To estimate the exponential integral we use the following bound:

$$\frac{1}{2} e^{-x} \ln\left(1 + \frac{2}{x}\right) < E_1(x) < e^{-x} \ln\left(1 + \frac{1}{x}\right), \quad (35)$$

where  $x > 0$ .

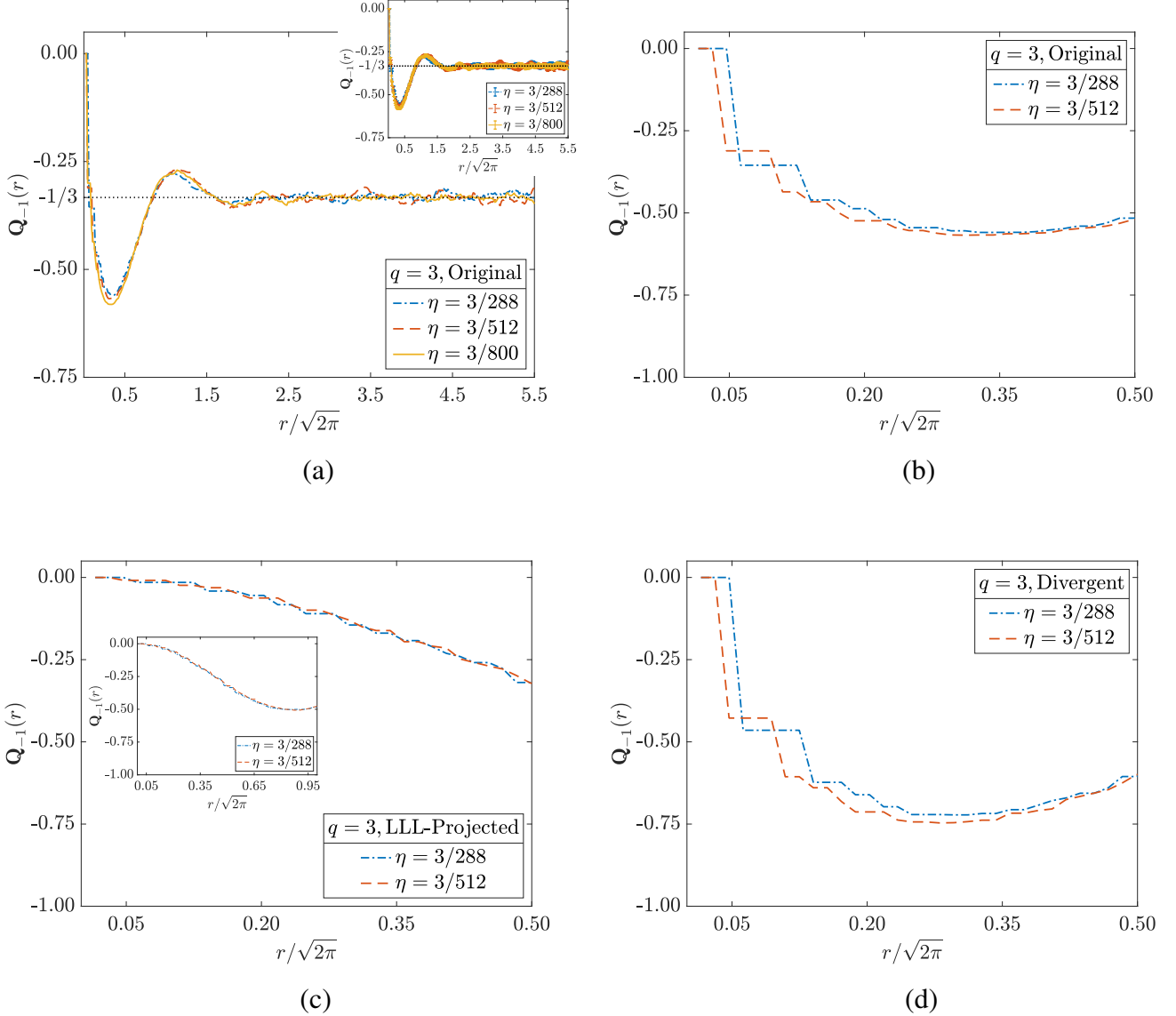


FIG. 6. The divergent terms in the expansion of Eq. (13) [the terms that are not confined to the LLL in the continuum – i.e., the ones left after subtracting Eq. (39) from (13)] are responsible for the changes in  $\mathbf{Q}_{-1}(r)$  between  $0 < r \lesssim \sqrt{2\pi}$ . All of these plots are for a square lattice on a circular disk of radius  $R \approx 8.3\sqrt{2\pi}$  and  $q = 3$ . We plot  $\mathbf{Q}_{-1}(r)$  vs.  $r$  with ansatz (13) for  $\eta = 3/288, 3/512$ , and  $3/800$  in (a). As we decrease  $\eta$ , the minimum of  $\mathbf{Q}_{-1}(r)$  near  $r = 0.25\sqrt{2\pi}$  keeps decreasing. The oscillations about  $\mathbf{Q}_{-1}(r) = -1/3$  for  $r \gtrsim 2.0\sqrt{2\pi}$  gradually decrease with decreasing  $\eta$ . We have included the  $\pm\sigma$  errorbars in the inset of (a). In (b), (c), and (d) we show the  $\mathbf{Q}_{-1}(r)$  vs.  $r$  plots for  $\eta = 3/288$  and  $3/512$ , where we compute the excess charges with the ansatz (13), with ansatz (13) projected to the LLL [i.e., with ansatz (39)], and with only the divergent terms in Eq. (13), respectively. From (c), we notice that  $\mathbf{Q}_{-1}(r)$  calculated with Eq. (39) for the two different values of  $\eta$  are almost identical. The inset of (c) shows  $\mathbf{Q}_{-1}(r)$  for upto  $r = \sqrt{2\pi}$ . In both (b) and (d), there are significant changes in  $\mathbf{Q}_{-1}(r)$  when  $\eta$  changes.

For comparing the contribution of the regular terms with the contribution of the irregular terms with poles, we introduce the following (always positive) ratio:

$$r = \frac{\mathcal{C}_{\infty}^2}{\mathcal{C}_{\text{reg}}^2} = \frac{1}{2}E_1\left(\frac{\xi^2}{2}\right)r_*(M), \quad (36)$$

where  $r_*(M)$  denotes a function of  $M$ . In the above, we have used that each term of the sum  $\sum_k$  in the right hand side of

Eq. (32b) is proportional to  $E_1(\xi^2/2)/2$ . From Eqs. (35) and (36), we show that in the continuum limit the contribution from the pole (32b) diverges as  $\ln N$ , when the quasielectron is situated either at the center of a square plaquette or midway between two lattice sites. The slow nature of the singularity is indeed difficult to capture in numerics.

Consistent with the above analysis, we numerically demonstrate that in the divergence of the excess charge  $\mathbf{Q}_{-1}(r)$  the

irregular terms (the ones leading to a pole in the continuum and hence not confined to the LLL) in ansatz (13) play the most important part. Here we are concerned about the continuous lowering of the  $\mathbf{Q}_{-1}(r)$  profile near the minima close to  $r = 0.25\sqrt{2\pi}$ . The other parts of the profile eventually converge. In particular, the oscillations for  $r \gtrsim 2.0\sqrt{2\pi}$  due to the underlying lattice structure die off, see Fig. 6a. With the help of Figs. 6b, 6c, and 6d we show that, when we decrease  $\eta$ , the  $\mathbf{Q}_{-1}(r)$  profile between  $0 < r \lesssim \sqrt{2\pi}$  is most affected by the aforementioned divergent terms.

## V. FAILURE OF THE LLL-PROJECTED QUASIELECTRON ANSATZ

The obvious way to remove the singularity at the quasielectron position  $w_1$  from the ansatz (13) is to project it to the LLL. We do this by removing the singular terms, which amounts to subtracting the following terms from  $\prod_{i<j} (z_i - z_j)^{qn_i n_j}$ :

$$\begin{aligned} \mathcal{R} = & \sum_{k=1}^N n_k \prod_{l(>k)} (w_1 - z_l)^{qn_l n_k} \\ & \times \prod_{l(<k)} (z_l - w_1)^{qn_k n_l} \prod_{\substack{i<j \\ i,j \neq k}} (z_i - z_j)^{qn_i n_j}. \end{aligned} \quad (37)$$

Comparing Eq. (37) with Eq. (29), we note that it is equivalent to subtracting the following from  $\prod_{i<j} (Z_i - Z_j)^q$  in the continuum limit:

$$\begin{aligned} \mathcal{R}_{\text{cont}} = & \sum_{k=1}^M \prod_{l(>k)} (w_1 - Z_l)^q \\ & \times \prod_{l(<k)} (Z_l - w_1)^q \prod_{\substack{i<j \\ i,j \neq k}} (Z_i - Z_j)^q. \end{aligned} \quad (38)$$

Using this we write the modified lattice ansatz for a single quasielectron as follows:

$$\begin{aligned} |\psi_{\text{QE}}\rangle = & \mathcal{C}^{-1} \sum_{n_1, \dots, n_N} \delta_n \prod_{i=1}^N \chi_{n_i} \prod_{i=1}^N (w_1 - z_i)^{-n_i} \\ & \times (1 - \mathcal{F}) \prod_{i<j} (z_i - z_j)^{qn_i n_j - \eta(n_i + n_j)} |n_1, \dots, n_N\rangle, \end{aligned} \quad (39)$$

where we use phase factors  $\chi_{n_i}$  similar to Eq. (12), and use the following definition for  $\mathcal{F}$ :

$$\begin{aligned} \mathcal{F} = & \mathcal{R} \prod_{i<j} (z_i - z_j)^{-qn_i n_j} \\ = & \sum_k n_k \prod_{l(\neq k)} \left( \frac{w_1 - z_l}{z_k - z_l} \right)^{qn_l n_k}. \end{aligned} \quad (40)$$

Incorporating the above modification, one writes the ansatz for a quasielectron at  $w_1$  and a quasihole at  $w_2$  as follows:

$$\begin{aligned} |\psi\rangle = & \mathcal{C}^{-1} \sum_{n_1, \dots, n_N} \delta_n \prod_{i=1}^N \chi_{n_i} \\ & \times \prod_{i=1}^N (w_1 - z_i)^{-n_i} (1 - \mathcal{F}) \prod_{i=1}^N (w_2 - z_i)^{n_i} \\ & \times \prod_{i<j} (z_i - z_j)^{qn_i n_j - \eta(n_i + n_j)} |n_1, \dots, n_N\rangle, \end{aligned} \quad (41)$$

where we have kept the multiplicative factor for the quasihole  $\prod_{i=1}^N (w_2 - z_i)^{n_i}$  unchanged.

We numerically study the excess charge profiles with the modified divergence-free quasielectron (39) in Fig. 7. It is known that for  $\eta = q/2$  the quasielectron excess charge is precisely the negative of the quasihole excess charge [17]. For this special value of  $\eta$  we see that the original quasielectron (13) and the modified divergence-free quasielectron (39) produce almost similar profiles for  $\mathbf{Q}_{-1}(r)$ . However, as we move away from this special  $\eta$  value and move toward the continuum limit, the difference between the two quasielectrons becomes more apparent. However, for large  $r$  we observe  $\mathbf{Q}_{-1}(r) \rightarrow 1/q$  for both quasielectrons. We now demonstrate that the LLL-projected quasielectron does not have the desired properties.

### A. Inconsistencies in the Modified Ansatz

In this section we first show that the modified ansatz fails to obtain correct braiding properties for the quasiparticles. We further demonstrate that starting from the ansatz for an FQH system with a quasihole and a modified quasielectron it is not possible to isolate a quasihole.

#### 1. Incorrect Braiding Statistics

To determine the braiding statistics between a quasihole and the modified quasielectron, we need to obtain the Berry phases from the wavefunction (41). We write the normalization constant there as follows:

$$\begin{aligned} \mathcal{C}^2 = & \sum_{n_1, \dots, n_N} \delta_n \prod_i |w_1 - z_i|^{-2n_i} |w_2 - z_i|^{2n_j} \\ & \times \prod_{i<j} |z_i - z_j|^{2qn_i n_j - 2\eta(n_i + n_j)} |1 - \mathcal{F}|^2. \end{aligned} \quad (42)$$

Following the same steps delineated in Sect. III A, we obtain the Berry phase by moving the quasihole coordinate  $w_2$  in a loop as follows:

$$\theta_2 = \frac{i}{2} \oint_c \sum_i \frac{\langle n_i \rangle}{w_2 - z_i} dw_2 + \text{c.c.}, \quad (43)$$

where we have used the fact that  $\mathcal{F}$  is  $w_2$  independent. Using this expression for the Berry phase, and the fact that both the quasihole and modified quasielectron are localized, we obtain

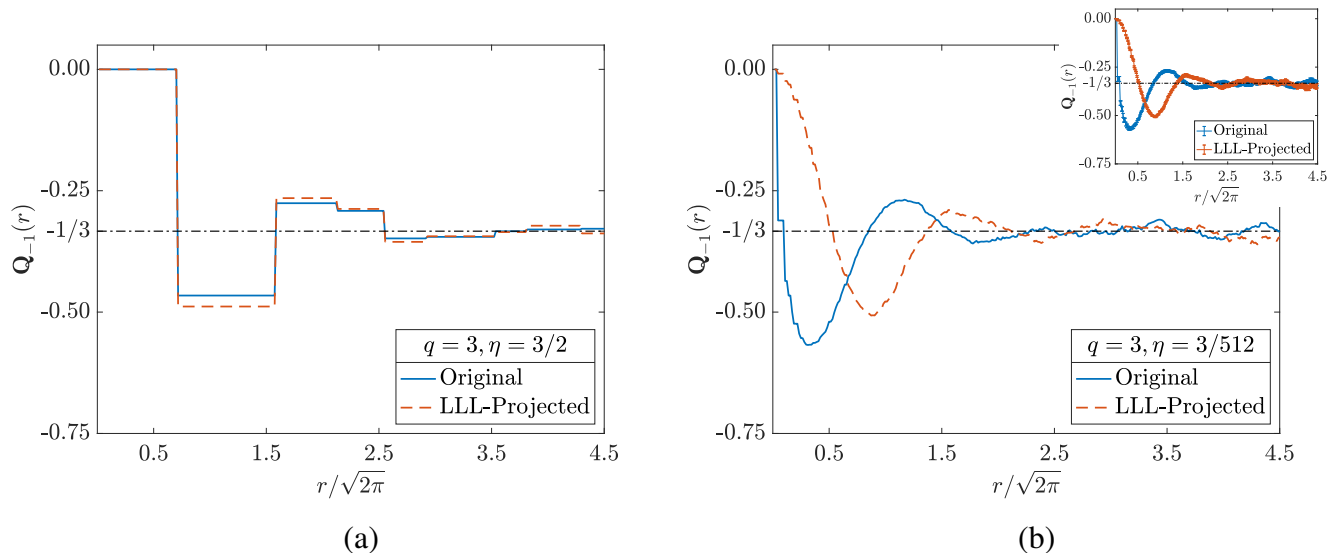


FIG. 7. Comparison of the excess charge  $\mathbf{Q}_{-1}(r)$  for the quasielectron, calculated with the original quasielectron ansatz (13) [blue solid] and the modified divergence-free ansatz (39) [red dashed]. Both of them are for a square lattice on a circular disk of radius  $R \approx 8.3\sqrt{2\pi}$  and inverse filling fraction  $q = 3$ . We have  $\eta = q/2$  in (a), and  $\eta = q/(2 \times 16^2)$  in (b) [ $\pm\sigma$  errorbar in the inset]. Already in (a) the excess charge profiles do not match fully. For large  $r$ , however, we observe that  $\mathbf{Q}_{-1}(r) \rightarrow 1/q$  for all the profiles.

the anyonic statistics between the quasihole and the quasielectron to be  $\gamma = -1/q$ .

We then proceed to calculate the Berry phase by moving the quasielectron coordinate  $w_1$  in a loop and obtain

$$\theta_1 = -\frac{i}{2} \oint_c \sum_i \frac{\langle n_i \rangle}{w_1 - z_i} dw_1 - \frac{i}{2} \oint_c \left\langle \frac{1}{1 - \mathcal{F}} \frac{\partial \mathcal{F}}{\partial w_1} \right\rangle dw_1 + c.c.. \quad (44)$$

Using this Berry phase does not derive the correct anyonic statistics because of the additional term. Moreover, this additional term contains nontrivial poles of  $w_1$  that are functions of the lattice positions  $z_i$ . As a result, it depends on the size and shape of the contour  $c$ . This failure renders the modified quasielectron ansatz (39) unusable.

## 2. Isolating a Quasihole

We explained above Eq. (13), how taking the limit  $w_2 \rightarrow \infty$  in Eq. (12) leads to an isolated quasielectron at  $w_1$ . One can similarly take the  $w_1 \rightarrow \infty$  limit. In Eq. (12),  $\prod_{i=1}^N (w_1 - z_i)^{-n_i}$  becomes a  $z_i$  independent factor  $w_1^{-M}$  in that limit, which is absorbed in the normalization. Evidently this limit isolates the quasihole at  $w_2$ .

We take the limit  $w_1 \rightarrow \infty$  in Eq. (41). We only need to investigate the behavior of  $[1 - \mathcal{F}]$ . Since  $w_1$  is in the nu-

merator of  $\mathcal{F}$ , we neglect the one in front. The problem is that this factor contains factors like  $(z_l - z_k)^{q n_l n_k}$ . Because of such dependence on  $z_1, \dots, z_N$ , we cannot absorb  $\mathcal{F}$  in the normalization.

## VI. CONCLUSION

In this paper, we studied the continuum limit of a lattice quasielectron ansatz. This lattice quasielectron, besides having the localization in the correct position and having the correct braiding properties, is the inverse of the lattice quasihole.

Our study reveals that a continuum limit of this lattice wavefunction does not exist. Only when the quasielectron is placed on top of a lattice site, this limit of the lattice quasielectron gives a finite result. Otherwise, depending on how we approach it, in the continuum limit the quasielectron pole gives rise to a slow  $\ln N$  singularity, where  $N$  is the number of lattice sites. This also explains why such divergence is hard to observe in the numerics. We then try to salvage the ansatz wavefunction by projecting it on the LLL, which removes the singularity. We demonstrate that the projected state fails to obtain the correct braiding properties. We hence conclude that taking the continuum limit of the lattice quasielectron wavefunction does not lead to a good continuum quasielectron ansatz.

## ACKNOWLEDGMENTS

We thank Maria Hermanns and Eddy Ardonne for several helpful discussions and comments on the manuscript.

- 
- [1] D. C. Tsui, H. L. Stormer, and A. C. Gossard, Two-dimensional magnetotransport in the extreme quantum limit, *Phys. Rev. Lett.* **48**, 1559 (1982).
- [2] D. Tong, Lectures on the Quantum Hall Effect, [arXiv:1606.06687](https://arxiv.org/abs/1606.06687) (2016).
- [3] A. Stern, Anyons and the quantum Hall effect – A pedagogical review, *Ann. Phys.* **323**, 204 (2008).
- [4] J. K. Jain, *Composite Fermions* (Cambridge University Press, Cambridge, 2007).
- [5] A. Yu. Kitaev, Fault-tolerant quantum computation by anyons, *Ann. Phys.* **303**, 2 (2003).
- [6] R. B. Laughlin, Anomalous quantum Hall effect: An incompressible quantum fluid with fractionally charged excitations, *Phys. Rev. Lett.* **50**, 1395 (1983).
- [7] R. B. Laughlin, *Elementary theory: The incompressible quantum fluid*, in *The quantum Hall effect* (Springer, New York, 1987).
- [8] G. S. Jeon and J. K. Jain, Nature of quasiparticle excitations in the fractional quantum Hall effect, *Phys. Rev. B* **68**, 165346 (2003).
- [9] B. Yang and F. D. M. Haldane, Nature of quasielectrons and the continuum of neutral bulk excitations in Laughlin quantum Hall fluids, *Phys. Rev. Lett.* **112**, 026804 (2014).
- [10] B. A. Bernevig and F. D. M. Haldane, Clustering properties and model wave functions for non-Abelian fractional quantum Hall quasielectrons, *Phys. Rev. Lett.* **102**, 066802 (2009).
- [11] T. H. Hansson, C.-C. Chang, J. K. Jain, and S. Viefers, Composite-fermion wave functions as correlators in conformal field theory, *Phys. Rev. B* **76**, 075347 (2007).
- [12] T. H. Hansson, M. Hermanns, and S. Viefers, Quantum Hall quasielectron in conformal field theory, *Phys. Rev. B* **80**, 165330 (2009).
- [13] T. H. Hansson, M. Hermanns, N. Regnault, and S. Viefers, Conformal field theory approach to Abelian and non-Abelian quantum Hall quasielectrons, *Phys. Rev. Lett.* **102**, 166805 (2009).
- [14] J. Suorsa, S. Viefers, and T. H. Hansson, A general approach to quantum Hall hierarchies, *New Journal of Physics* **13**, 075006 (2011).
- [15] M. Greiter, V. Schnells, and R. Thomale, Laughlin states and their quasiparticle excitations on the torus, *Phys. Rev. B* **93**, 245156 (2016).
- [16] J. Kjäll, E. Ardonne, V. Dwivedi, M. Hermanns, and T. H. Hansson, Matrix product state representation of quasielectron wave functions, *J. Stat. Mech.* **2018**, 053101 (2018).
- [17] A. E. B. Nielsen, I. Glasser, and I. D. Rodríguez, Quasielectrons as inverse quasiholes in lattice fractional quantum Hall models, *New J. Phys.* **20**, 033029 (2018).
- [18] T. Neupert, L. Santos, C. Chamon, and C. Mudry, Fractional quantum Hall states at zero magnetic field, *Phys. Rev. Lett.* **106**, 236804 (2011).
- [19] N. Regnault and B. Andrei Bernevig, Fractional Chern insulator, *Phys. Rev. X* **1**, 021014 (2011).
- [20] E. J. Bergholtz and Z. Liu, Topological flat band models and fractional Chern insulators, *Int. J. Mod. Phys. B* **27**, 1330017 (2013).
- [21] H.-H. Tu, A. E. B. Nielsen, J. I. Cirac, and G. Sierra, Lattice Laughlin states of bosons and fermions at filling fractions  $1/q$ , *New J. Phys.* **16**, 033025 (2014).
- [22] A. E. B. Nielsen, Anyon braiding in semianalytical fractional quantum Hall lattice models, *Phys. Rev. B* **91**, 041106(R) (2015).
- [23] I. D. Rodríguez and A. E. B. Nielsen, Continuum limit of lattice models with Laughlin-like ground states containing quasiholes, *Phys. Rev. B* **92**, 125105 (2015).
- [24] M. Abramowitz and I. Stegun, *Handbook of mathematical functions with formulas, graphs, and mathematical tables* (United States Department of Commerce, National Bureau of Standards (NBS), 1964).